Macromolecules

ARTICLE

pubs.acs.org/Macromolecules

Order−Order Transition in a Rod−Coil Diblock Copolymer Induced by Supercritical CO_2

Ling-Ying Shi, Zhihao Shen,* and Xing-He Fan*

Beijing National Laboratory for Molecular Sciences, Key Laboratory of Polymer Chemistry and Physics of Ministry of Education, College of Chemistry and Molecular Engineering, Peking University, Beijing 100871, China

Supporting Information

ABSTRACT: We synthesized a series of well-defined rod−coil block copolymers (BCPs), poly(dimethylsiloxane)-*b*-poly{2,5-bis[(4-methoxyphenyl)oxycarbonyl]styrene} (PDMS-*b*-PMPCS), containing a CO_2-philic block PDMS, and we studied their phase structures in bulk and after treatment with supercritical CO_2 ($scCO_2$) using small-angle X-ray scattering. The nanostructure of the BCP changed from lamellae (LAM) to hexagonally packed cylinders (HEX) when the volume fraction of PDMS (f_{PDMS}) decreased to ∼18%. Although the glass transition temperature (T_g) of the PMPCS block in $scCO_2$ could not be measured directly in our experiment, it significantly decreased in $scCO_2$ at 110 bar as estimated from SAXS results. More significantly, we observed a HEX−LAM order−order transition induced by $scCO_2$ in a HEX-structured BCP which was located close to the HEX−LAM phase boundary in the BCP phase diagram under our experimental conditions. The OOT could be attributed to increases in both the volume fraction of the coil block and the effective interaction parameter. The lamellar structure was fixed by the rigid-rod-like block during depressurization. It was stable below the high T_g of the rod block and could change back to the original HEX structure by thermal annealing above the T_g of the rod block. For other BCPs which were located far away from the HEX−LAM phase boundary, the structures did not change, but the periodic sizes increased following $scCO_2$ treatment.

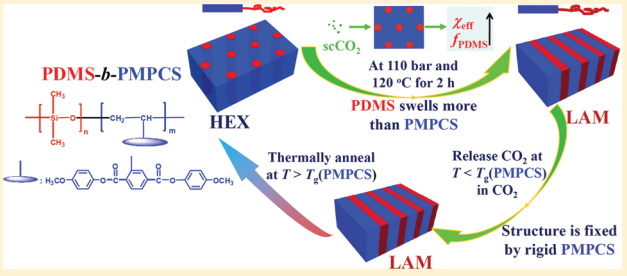

INTRODUCTION

The self-assembly of block copolymers (BCPs) in bulk state has been intensively studied for many years because it can provide a variety of periodic nanostructures which have important potential applications in nanotechnology.[1−5] Depending on the volume fraction f of the individual block and χN, where χ is the Flory−Huggins interaction parameter and N the total degree of polymerization of the copolymer, the nanostructures of diblock copolymers can be lamellae (LAM), hexagonally packed cylinders (HEX), bicontinuous gyroid, or cubic arrays of spheres.[6] Some other morphologies have been observed in rod−coil diblock copolymers, such as zigzag lamellae, wavy lamellae,[7] hexagonally perforated lamellae, and tetragonally perforated layers.[3,8] Moreover, among the ordered nanostructures, a variety of order−order transitions (OOTs) can be induced.

The reported OOTs of BCPs are always induced by the addition of selective solvents[9−11] or homopolymers,[12−14] alteration of temperature,[15,16] and application of special external fields, such as shear flow, electric fields, and magnetic fields.[17−19] However, the addition of homopolymers, unfortunately, has the disadvantage of producing more defects caused by the aggregation of the homopolymers.[20] Whereas the phases formed through thermally induced OOTs always only exist in a special temperature range, they revert to the original states when temperature returns, as in the thermoreversible OOT between the body-centered cubic spheres and the hexagonally packed cylinders in the polystyrene-*b*-polyisoprene diblock copolymer.[15] Applying external fields is another important choice for producing OOTs. Nevertheless, most reports about the effect of external fields on self-assembly of BCPs focus on improving the ordering and orientation, especially in thin films, except limited reports on OOTs induced by shear flow and electric fields. In a word, transitions among ordered phases are not easy to achieve, and the formed phases may change in some cases. For example, after the gyroid−cylinder transition of a polystyrene-*b*-polyisoprene diblock copolymer under the influence of a high electric field, the cylinder phase reverted to the gyroid one following the switch-off of the electric field.[21] Therefore, how to obtain OOTs easily while maintaining the stability of the final phase still remains a challenge for the further research of self-assembly in BCPs.

Alternatively, supercritical carbon dioxide ($scCO_2$), an attractive green solvent which is cheap, nontoxic, volatile, inert, nonflammable, and recyclable,[22,23] has potential benefits for structure control of BCPs. Although it is a poor solvent for most polymers, it is a relatively good solvent for amorphous fluoropolymers and polysilicones of moderate molecular weights,[24,25] and it is a plasticizer for most polymers and can decrease glass

Received: October 18, 2010
Revised: February 24, 2011
Published: March 24, 2011

dx.doi.org/10.1021/ma1023704 | *Macromolecules* 2011, 44, 2900–2907

transition temperatures (T_g's) dramatically.[26] The effects of $scCO_2$ on the phase behavior of bulk BCPs and polymer blends with each composition having weak interactions with $scCO_2$ have been investigated.[27−30] The results indicate that the temperatures of both enthalpy-driven upper order−disorder transitions and entropy-driven lower disorder−order transitions decrease in $scCO_2$. For BCPs with only one CO_2-philic block, the effect of $scCO_2$ on the phase behavior is complicated because of both the change of volume fraction f owing to selective swelling and the change of the interaction parameter χ due to the difference in polymer−CO_2 interaction parameters.[31] There is exacerbating entropic penalty for mixing as well as increased possibility for phase separation because of rapid and disparate increases in the free volumes of the copolymer components owing to the preferential sorption of $scCO_2$.[28] In addition, for self-assembly of diblock copolymer thin films, $scCO_2$ can improve the ordering of well-defined nanostructures, which can not be achieved by changing common solvents or by annealing in vacuum or in air.[32−34] For instance, PS-*b*-PFMA block copolymer thin films, which form fat cylinders from inverse micelles or have no ordered nanostructures depending on the initial casting solvents, change to vertically or horizontally aligned polymeric nanosheets after $scCO_2$ treatment.[35] And $scCO_2$ can be used to fabricate nanocellular structures and nanopores in block copolymer thin films.[36−38] However, to the best of our knowledge, there have been no reports about OOTs induced by $scCO_2$ in bulk rod−coil BCPs.

In this work, we synthesized a series of poly(dimethylsiloxane)-*b*-poly{2,5-bis[(4-methoxyphenyl)oxycarbonyl]styrene} (PDMS-*b*-PMPCS) block copolymers with polysiloxane as the CO_2-philic coil block and a mesogen-jacketed liquid crystalline polymer (MJLCP) as the CO_2-phobic rod block through atom transfer radical polymerization (ATRP). We studied the bulk phase behavior before and after $scCO_2$ treatment by small-angle X-ray scattering (SAXS) and found that when the block copolymer which had the nanostructure of hexagonally packed cylinders but was located close to the HEX−LAM phase boundary in the BCP phase diagram under our experimental conditions was subjected to $scCO_2$ treatment at appropriate pressures and temperatures, the HEX transformed into a LAM. As far as we know, this is the first report of a clear HEX−LAM transition in a rod−coil BCP in bulk induced by $scCO_2$. In addition, the final lamellar structure was stable when the temperature was below the T_g of the PMPCS block, and it could return to the HEX through thermal annealing.

EXPERIMENTAL SECTION

Materials. 2-Bromo-2-methylpropionyl bromide (Acros, 98%), monohydroxy-terminated poly(dimethylsiloxane) (PDMS-OH, Aldrich, 4670 g/mol, 0.97 g/cm^3), and *N*,*N*,*N*′,*N*″,*N*″-pentamethyldiethylenetriamine (PMDETA, TCI, 98%) were used as received. Triethylamine (98%) and tetrahydrofuran (THF, Beijing Chemical Reagents Co., A.R.) were used after distilled. Chlorobenzene was purified by washing with concentrated sulfuric acid to remove residual thiophenes, followed by washing with a 5% sodium carbonate solution and with water, and then dried with anhydrous calcium chloride and finally distilled. CuBr (Beijing Chemical Reagents Co., A.R.) was purified by washing with acetic acid, followed by washing with methanol, and then dried for use.

Synthesis of the Macroinitiator 2-Bromoisobutyrate-Terminated PDMS (PDMS-Br). PDMS-OH (10 g, 2.14 mmol) and triethylamine (0.433 g, 4.28 mmol) were dissolved in THF (100 mL), and 2-bromo-2-methylpropionyl bromide (0.984 g, 4.28 mmol) was first dissolved in THF (50 mL) and then added dropwise slowly. The reaction mixture was cooled in an ice/water bath and stirred at 0 °C for 1 h and then at room temperature for 10 h. The filtered solution was concentrated, dissolved in dichloromethane, washed with a saturated $NaHCO_3$ water solution for five times, and then dried by anhydrous magnesium sulfate for 30 min. The solvents were evaporated, and the purified PDMS-Br was easily obtained by drying in vacuum. Yield: 7.5 g (75%). The ^{1}H NMR spectra of PDMS-OH and PDMS-Br are shown in Figure S1 of the Supporting Information (SI). Characteristic peaks of PDMS-Br compared with that of PDMS-OH in ^{1}H NMR (300 MHz, $CDCl_3$, δ, ppm): 1.94 (s, 6H, $Br(CH_3)_2CCOOCH_2$), 3.43−3.46 (t, 2H, CH_2CH_2O), 3.65−3.68 (t, 2H, OCH_2CH_2O), 4.30−4.33 (t, 2H, CH_2CH_2OOC). The peaks of the protons near the hydroxy group of PDMS-OH shifted to low field after the reaction with 2-bromo-2-methylpropionyl bromide, indicating the success of the reaction. The appearance of a single peak at 1.94 ppm confirmed that the 2-bromoisobutyrate group was the end group of PDMS.

Fractionation of the Macroinitiator PDMS-Br. PDMS-Br synthesized from PDMS-OH had a broad and asymmetric molecular weight distribution with a polydispersity of 1.31. In order to synthesize structurally well-defined diblock copolymers, it was necessary to fractionate the macroiniator. With THF as the good solvent and methanol as the poor solvent, the fractionation was a process of gradual precipitation. The raw material was first dissolved in THF, and then methanol was added dropwise, leading to the precipitation of molecules with high molecular weights. The final product used as the initiator had a narrow molecular weight distribution as demonstrated by gel permeation chromatography (GPC, see Figure S2 and Table S3 in the SI) and matrix-assisted laser desorption/ionization time-of-flight mass spectrometry (MALDI-TOF MS, see Figure S3 in the SI) results.

Synthesis of PDMS-*b*-PMPCS by ATRP. In a typical experiment for polymerization, the monomer {2,5-bis[(4-methoxyphenyl)oxycarbonyl]styrene} (MPCS) (0.504 g, 1.25 mmol), PDMS-Br (0.1 g, 23 μmol), CuBr (3.31 mg, 23 μmol), PMDETA (3.99 mg, 23 μmol), and chlorobenzene (3.05 mL) were charged into a polymerization tube. After stirred and degassed by three freeze−pump−thaw cycles, the tube was sealed under vacuum and subsequently immerged into an oil bath thermostated at 90 °C for 8 h. It was then quenched in liquid nitrogen and taken out to ambient condition. The solution was passed through a neutral alumina column in order to remove copper salt. Finally, the copolymer was precipitated in a large volume of methanol and dried in vacuum overnight. Figure S4 in the SI is the representative ^{1}H NMR spectrum of the PDMS-*b*-PMPCS block copolymers. The resonance signals of protons of the methyl group in PDMS (a), vinyl backbone (b and b′), methyl group (c), disubstituted phenyl (d), and trisubstituted phenyl (e) in PMPCS appeared at δ = −0.05−0.20, 1.52−1.82, 3.40−3.89, 6.38−6.96, and 7.2−7.82 ppm, respectively.

Supercritical CO_2 Treatment. The sample was placed in a stainless steel high-pressure vessel (Parr Series 4560 mini bench top reactor) which was later filled with high-pressure CO_2, and the vessel was heated to a certain temperature (controlled by Parr Model 4843 temperature controller) and annealed for 2 h at a constant pressure. Then the vessel was placed in an ice/water bath to quench the sample, and CO_2 was released at a rate of ∼20 bar/min.

Characterization Techniques. The molecular weights of macroinititor and BCPs were determined with the combination of GPC, MALDI-TOF MS measurements, and elemental analyses (EA). GPC experiments were conducted on a Waters 2410 instrument equipped with a Waters 2410 RI detector, with pure THF as eluent (1.0 mL/min). The calibration curve was obtained with linear polystyrenes as standards. ^{1}H NMR spectra were obtained with a Bruker 400 MHz spectrometer. MALDI-TOF MS measurements were performed on a Bruker Autoflex high-resolution tandem mass spectrometer. Differential scanning calorimetry (DSC) measurements were carried out on a TA Q100 DSC

Scheme 1. Synthesis of PDMS-*b*-PMPCS Block Copolymers

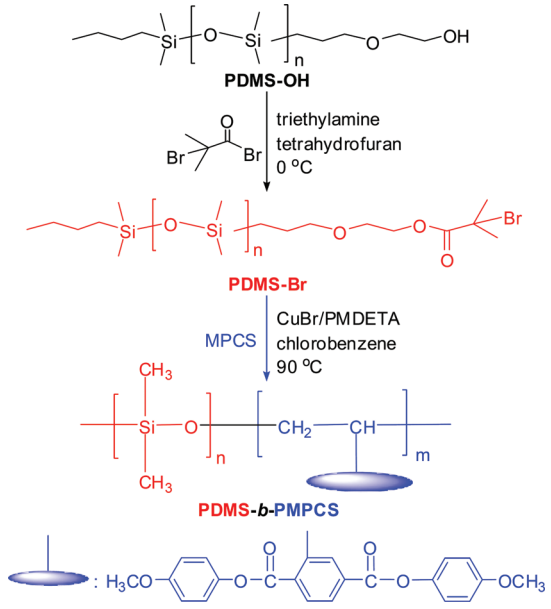

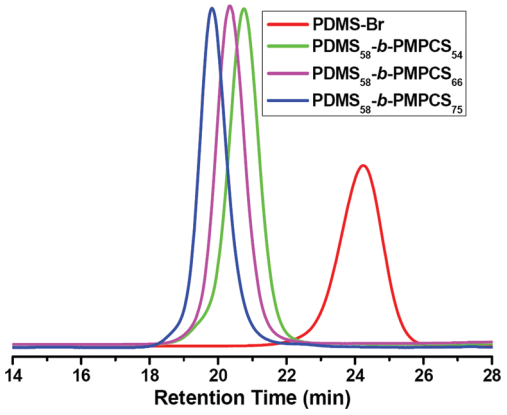

Figure 1. GPC curves of the macroinitiator and the block copolymers synthesized.

calorimeter in a nitrogen atmosphere. SAXS experiments were carried out on a Bruker Nanostar SAXS instrument using Cu Kα radiation at a wavelength of 0.154 nm. The working voltage and current were 40 kV and 650 μA, respectively. The scattering vector q is defined as $q = 4\pi/\lambda \sin\theta$, where the scattering angle is 2θ, and the d-spacing (d) is given by $2\pi/q$.

RESULTS AND DISCUSSION

Synthesis and Characterization of PDMS-*b*-PMPCS BCPs. As shown in Scheme 1, a series of PDMS-*b*-PMPCS BCPs with different molecular weights were synthesized through ATRP initiated by the same PDMS macroinitiator prepared from commercially available PDMS-OH. The macroinitiator, PDMS-Br, was synthesized through the reaction between PDMS-OH and 2-bromoisobutyryl bromide and was then fractionated to have a low polydispersity. Pure PDMS-Br after fractionation was characterized by ^{1}H NMR (Figure S1 in SI), GPC (Figure S2 and Table S3 in SI), EA (Table S4 in SI), and MALDI-TOF MS (Figure S3 in SI). The number-average molecular weight and polydispersity index (PDI) of PDMS-Br were 4332 g/mol and 1.02, respectively, from MALDI-TOF MS results. The monomer of the PMPCS block, MPCS, was prepared and characterized as described in the literature.[39] Using PDMS-Br as initiator, CuBr as catalyst, PMDETA as ligand, and chlorobenzene as solvent, a variety of PDMS-*b*-PMPCS diblock copolymers were synthesized by changing the ratio of macroinitiator to monomer. All PDMS-*b*-PMPCS BCPs were characterized by ^{1}H NMR (Figure S4 in SI), EA (Table S4 in SI), and GPC (Figure 1 and Table 1). The molecular weights ranged from 13 800 to 20 100 g/mol from GPC results. The volume fraction of PDMS (f_{PDMS}) was 20.7−15.8% calculated from the MALDI-TOF MS result of the macroinitiator and the EA results of the BCPs using densities of 0.97 g/cm^3 for PDMS (provided by supplier) and 1.28 g/cm^3 for PMPCS in the literature[40] (Table 1). All results indicated that these block copolymers had well-defined chemical structures with symmetric and narrow molecular weight distributions.

Phase Structures of PDMS-*b*-PMPCS BCPs in Bulk. The microphase separation of originally amorphous BCPs always occurs above the T_g's of all blocks. The T_g of PDMS is known to be low at about −120 °C. Therefore, the T_g of PMPCS is the key for the microphase separation. The T_g of PMPCS in all BCPs determined by DSC was almost the same at 113−118 °C, as listed in Table 1. The phase structures of the PDMS-*b*-PMPCS BCPs were determined by SAXS experiments. All the samples were annealed in vacuum at 160 °C for 10 h before SAXS measurements. The SAXS profiles are shown in Figure 2, and the q^* and calculated d-spacing values of the peaks are shown in Table 1. The peaks in the scattering profile of PDMS$_{58}$-*b*-PMPCS$_{54}$ had a scattering vector ratio of 1:2:3:4, which was characteristic of a lamellar structure. The primary reflection was at q^* = 0.253 nm^{-1} corresponding to a d-spacing of 24.8 nm. Different from coil−coil BCPs, this rod−coil BCP still had a lamellar structure even with a rather unsymmetrical composition. The peaks in the scattering profiles of PDMS$_{58}$-*b*-PMPCS$_{66}$ and PDMS$_{58}$-*b*-PMPCS$_{75}$ had a scattering vector ratio of $1:\sqrt{3}:\sqrt{7}:\sqrt{13}$, which was characteristic of hexagonally packed cylinders. The SAXS profiles of hexagonally packed cylinders lacked the high-order reflection with a q value of $\sqrt{4}q^*$ because of the small volume fractions of the cylinder phase in PDMS$_{58}$-*b*-PMPCS$_{66}$ and PDMS$_{58}$-*b*-PMPCS$_{75}$ (ϕ_{PDMS} < 18%).[41,42] The primary reflections were at q^* = 0.223 and 0.186 nm^{-1}, corresponding to d-spacing values of 28.2 and 33.8 nm, respectively. These results indicated that the self-assembled nanostructures of PDMS-*b*-PMPCS changed from lamellae to hexagonally packed cylinders as the volume fraction of PDMS decreased.

It was necessary to explain why we chose 160 °C as the annealing temperature. In-situ SAXS measurements on PDMS$_{58}$-*b*-PMPCS$_{66}$ during heating were first carried out to determine the influence of temperature on the BCP phase behavior in bulk. As shown in Figure 3, although the first scattering peak of the sample appeared at 120 °C which was just slightly above the T_g of PMPCS (116 °C), the higher-order reflection peaks that indicated the formation of ordered nanostructures appeared when the temperature was above 150 °C, which was ascribed to the fact that the development of ordered structures of the BCPs containing rodlike MJLCPs was related not only to the T_g's but also to the temperatures at which the liquid crystalline (LC) phases of MJLCPs formed as described in the literature.[43] The LC formation temperatures of PDMS$_{58}$-*b*-PMPCS$_{54}$, PDMS$_{58}$-*b*-PMPCS$_{66}$, and PDMS$_{58}$-*b*-PMPCS$_{75}$ were about 160, 150, and

Table 1. Molecular Weights, Polydispersity Indexes, f_{PDMS} and T_g Values of the Macroinitiator and the Diblock Copolymers, and Nanostructure Characteristics of the Diblock Copolymers from SAXS Results

sample	M_n[a] (g/mol)	M_n[b] (g/mol)	PDI[a]	f_{PDMS}[b] (%)	T_g[c] (°C)	q^* (nm^{-1})	d (nm)	nanostructure
PDMS-Br	4 300	4 500	1.07	100				
$PDMS_{58}$-*b*-$PMPCS_{54}$	13 800	26 100	1.07	20.7	113	0.253	24.8	LAM
$PDMS_{58}$-*b*-$PMPCS_{66}$	16 400	31 100	1.07	17.5	116	0.223	28.2	HEX
$PDMS_{58}$-*b*-$PMPCS_{75}$	20 100	34 500	1.06	15.8	118	0.186	33.8	HEX

[a] Determined from GPC results using linear polystyrene standards. [b] Determined from MALDI-TOF MS of PDMS-Br and EA results of the block copolymers. [c] Determined from DSC results.

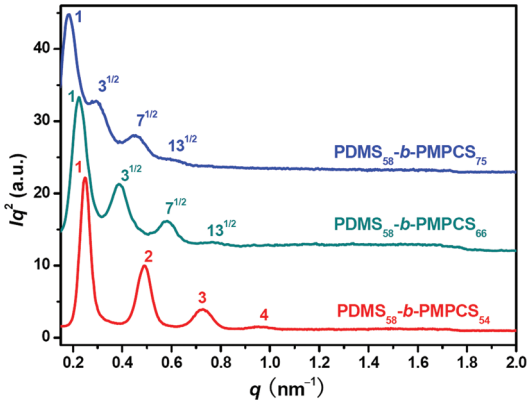

Figure 2. SAXS profiles of PDMS-*b*-PMPCS diblock copolymers after annealing in vacuum at 160 °C for 10 h.

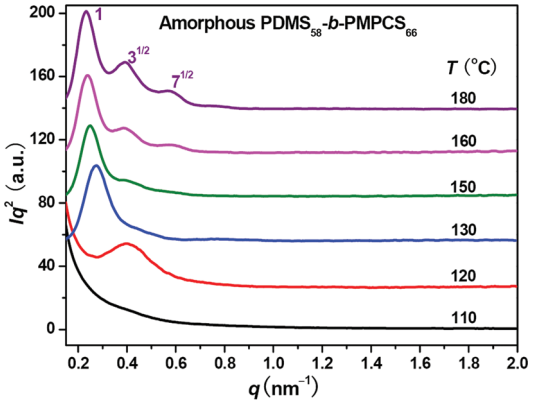

Figure 3. SAXS profiles of $PDMS_{58}$-*b*-$PMPCS_{66}$ at different temperatures indicated after it was annealed at the same temperatures for 2 h during heating.

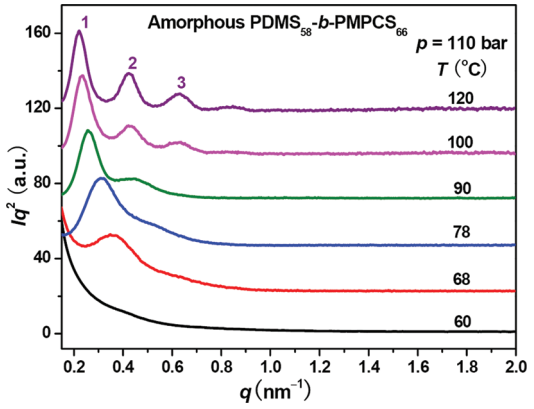

Figure 4. SAXS profiles of $PDMS_{58}$-*b*-$PMPCS_{66}$ at ambient temperature after $scCO_2$ treatment at 110 bar and at different temperatures indicated for 2 h.

140 °C, respectively. Moreover, the thermal SAXS results of $PDMS_{58}$-*b*-$PMPCS_{66}$ indicated that its nanostructure was still HEX after thermal annealing even at temperatures higher than 200 °C.

Estimation of T_g of the PMPCS Block of $PDMS_{58}$-*b*-$PMPCS_{66}$ in $scCO_2$. The T_g's of block polymers in $scCO_2$ decrease dramatically, which plays an important role in the effect of $scCO_2$ on BCP phase behavior as repored in the literature.[26] Moreover, the T_g of a BCP in $scCO_2$ is a key parameter of structure control in $scCO_2$ processing. It was difficult to directly measure the T_g of PMPCS in $scCO_2$ in situ in our experiments. However, we estimated the T_g of the PMPCS block of $PDMS_{58}$-*b*-$PMPCS_{66}$ in $scCO_2$ by comparing the results of thermal SAXS experiments on the originally amorphous sample with those on samples that were treated by $scCO_2$ at a constant pressure of 110 bar but at different temperatures, taking advantage of the fact that the first scattering peak appeared when the annealing temperature was just above the T_g of PMPCS, as demonstrated in Figure 3. The annealing time during heating at each temperature was 2 h, and the time of $scCO_2$ treatment was also 2 h. The samples after $scCO_2$ treatment were quenched to about 30 °C with an ice/water bath before depressurization. The SAXS profiles are shown in Figure 4. The primary scattering peak appeared after $scCO_2$ treatment at 68 °C, which indicated that the T_g of the PMPCS block of $PDMS_{58}$-*b*-$PMPCS_{66}$ in $scCO_2$ at 110 bar was 61−67 °C. Because the T_g's of PMPCS of the other two BCPs were almost the same as that of $PDMS_{58}$-*b*-$PMPCS_{66}$, the T_g's of the PMPCS block of these BCPs in $scCO_2$ at 110 bar were also similar. And the samples were quenched to temperatures lower than 50 °C before depressurization in the following $scCO_2$-treating experiments in order to preserve the swollen structures.

Furthermore, the high-order scattering peaks started to appear at 90 °C in Figure 4. This temperature was about 60 °C lower than that observed at atmospheric pressure as shown in Figure 3, which suggested that the temperature at which the LC phase started to develop also decreased in $scCO_2$.

HEX−LAM Transition and Size Dilation of PDMS-*b*-PMPCS BCPs after $scCO_2$ Treatment. The thermal SAXS results on $PDMS_{58}$-*b*-$PMPCS_{66}$ shown in Figure 3 indicated that the ordered structure was always HEX. And the SAXS results on originally amorphous, $scCO_2$-treated $PDMS_{58}$-*b*-$PMPCS_{66}$ in Figure 4 showed that high-order reflection peaks appeared when the sample was treated in $scCO_2$ at 100 °C and the scattering peaks had a scattering vector ratio of 1:1.85:2.78, which might be attributed to the existence of both lamellae and hexagonally

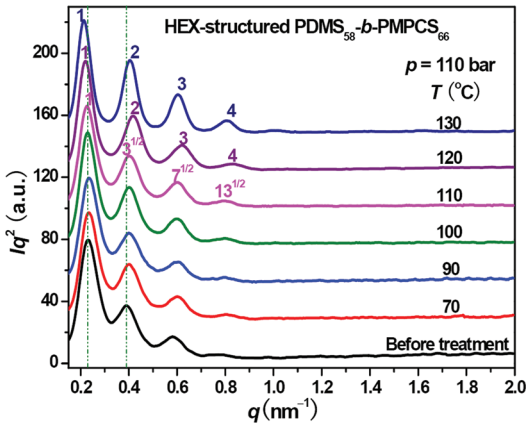

Figure 5. SAXS profiles of HEX-structured $PDMS_{58}$-*b*-$PMPCS_{66}$ after $scCO_2$ treatment at different temperatures indicated and at a constant pressure of 110 bar.

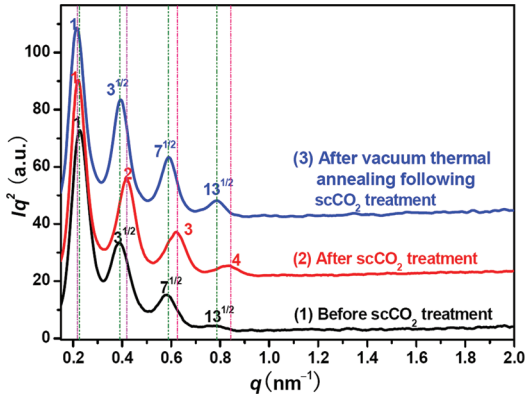

Figure 6. SAXS profiles of $PDMS_{58}$-*b*-$PMPCS_{66}$: before $scCO_2$ treatment (curve 1), after $scCO_2$ treatment at 120 °C and 110 bar (curve 2), and after vacuum thermal annealing following $scCO_2$ treatment (curve 3).

packed cylinders. On the other hand, when the originally amorphous sample was treated by $scCO_2$ at 120 °C, the reflection peaks in the scattering profile had a scattering vector ratio of 1:2:3, indicating the formation of a lamellar structure. The annealing of amorphous $PDMS_{58}$-*b*-$PMPCS_{66}$ in vacuum or $scCO_2$ resulted in different nanostructures. The next question was what would happen to $PDMS_{58}$-*b*-$PMPCS_{66}$ with a HEX structure by $scCO_2$ treatment.

PDMS is CO_2-philic. Therefore, we supposed that when the PDMS-*b*-PMPCS diblock copolymer which had a structure of hexagonally packed cylinders but was located close to the HEX-LAM phase boundary in the BCP phase diagram under our experimental conditions was subjected to $scCO_2$ treatment, the nanostructure could be greatly influenced. We treated the $PDMS_{58}$-*b*-$PMPCS_{66}$ with a structure of hexagonally packed cylinders using $scCO_2$ at different temperatures from 70 to 130 °C at a constant pressure of 110 bar. The samples after treatment were characterized by SAXS (Figure 5). Although the high-order reflection peaks slightly shifted to higher q values after $scCO_2$ treatment below 110 °C, the scattering vector ratio of the peaks had no distinct change. However, the primary peak shifted to a lower q, but the other peaks shifted to higher q's after $scCO_2$ treatment at 120 or 130 °C, resulting in a scattering vector ratio of 1:2:3:4 within experimental errors instead of

Table 2. Morphological Characteristics of $PDMS_{58}$-*b*-$PMPCS_{66}$ from SAXS Results

sample	q^* (nm^{-1})	d (nm)	nanostructure
before $scCO_2$ treatment	0.223	28.2	HEX
after $scCO_2$ treatment	0.218	28.8	LAM
after vacuum thermal annealing following $scCO_2$ treatment	0.220	28.5	HEX

1:$\sqrt{3}$:$\sqrt{7}$:$\sqrt{13}$, indicating that the hexagonally packed cylinders transformed into lamellae completely (as shown in Figure 6 and Table 2).

In addition, we treated $PDMS_{58}$-*b*-$PMPCS_{66}$ under other conditions. When the temperature was above 120 °C at 110 bar, or the pressure was above 110 bar at 120 °C, the similar HEX−LAM OOT occurred (Figure S5 in SI). And we also treated the sample at a lower temperature but at a higher pressure. The results indicated that when the temperature was 110 °C, the order−order transition could occur at 160 bar (Figure S5 in SI). Moreover, the LC phase structure of PMPCS did not change after $scCO_2$ treatment in our experimental conditions for inducing OOTs. The OOT described in this work was different from the transformation of PS-*b*-PFMA block copolymer thin films to lamellar structures, where the original structures of the copolymer were not truly well ordered hexagonally packed cylinders.[35] And the selective swelling of PDMS in the coil−coil PS-*b*-PDMS BCP described in the literature had no order−order transition irrespective of the temperature (40−140 °C) or pressure (<250 bar).[44]

The lamellar phase of $PDMS_{58}$-*b*-$PMPCS_{66}$ transformed from hexagonally packed cylinders was stable at temperatures below the T_g of PMPCS. We verified the structure by SAXS in 6 weeks after $scCO_2$ treatment, and the scattering profile was still the same as that of the sample immediately after $scCO_2$ treatment. However, the LAM was still possible to return to hexagonally packed cylinders. When the $scCO_2$-treated lamellar $PDMS_{58}$-*b*-$PMPCS_{66}$ was annealed in vacuum at 160 °C for 10 h again, the morphology reverted to hexagonally packed cylinders, which was demonstrated by the SAXS result in Figure 6 (curve 3).

From the phase diagram of a BCP, an order−order transition can occur when there is a large enough change in either the volume fraction f or the Flory−Huggins interaction parameter χ. On one hand, the OOT in this work could be attributed to the greater swelling of PDMS in $scCO_2$, leading to an increase in the effective volume fraction of PDMS. Therefore, the phase was inclined to develop into lamellae from the hexagonally packed cylinders. When CO_2 was released, there might be some void space left in the final structure, and the periodic size would increase. Although the d-spacing of the new lamellar phase was different from that of the original hexagonally packed cylinders, the periodic sizes of these two phases could not be compared directly. In order to confirm our conjecture, we studied the effect of $scCO_2$ on $PDMS_{58}$-*b*-$PMPCS_{54}$ and $PDMS_{58}$-*b*-$PMPCS_{75}$ in the same way. After $scCO_2$ treatment at 120 °C and 110 bar, the structure of $PDMS_{58}$-*b*-$PMPCS_{54}$ was still lamellae, with about 1.0 nm size dilation (Figure 7a and Table 3). For $PDMS_{58}$-*b*-$PMPCS_{75}$ after treatment, the structure remained as hexagonally packed cylinders but was more ordered as evidenced by the more intense high-order diffraction peaks in the profile of the sample after treatment, with about 1.9 nm increase in d-spacing

dx.doi.org/10.1021/ma1023704 |*Macromolecules* 2011, 44, 2900–2907

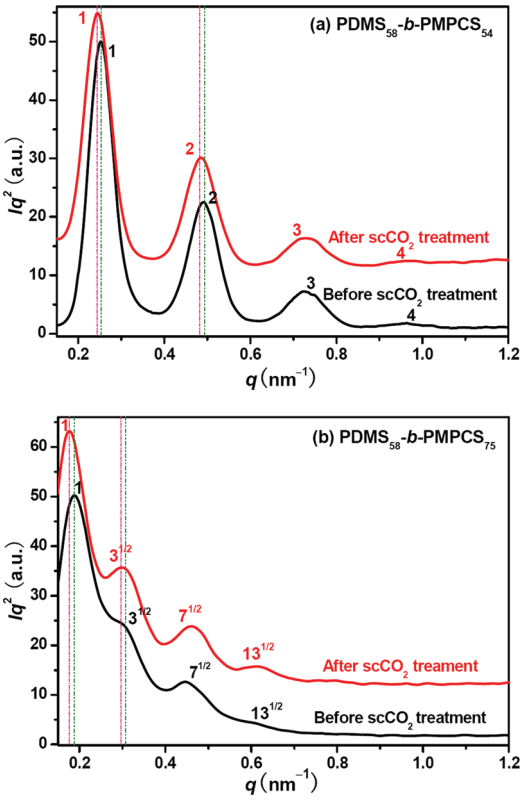

Figure 7. SAXS profiles of $PDMS_{58}$-*b*-$PMPCS_{54}$ (a) and $PDMS_{58}$-*b*-$PMPCS_{75}$ (b) before and after $scCO_2$ treatment at 120 °C and 110 bar for 2 h.

(Figure 7b and Table 3). Again, the size dilation could be ascribed to the void space produced in the block copolymers after depressurization, which was confirmed by the decreases in densities of the BCPs after $scCO_2$ treatment as described in the SI (Table S2). These results confirmed that the more swelling of PDMS was indeed an important reason for influencing the phase behavior and inducing the OOT of $PDMS_{58}$-*b*-$PMPCS_{66}$.

Variation of the Effective Interaction Parameter (χ_{eff}) in $scCO_2$ Processing. On the other hand, when PDMS-*b*-PMPCS was swollen by $scCO_2$, as in a strong selective solvent, the χ_{eff} changed to

$$\chi_{eff} \sim \phi(\chi_{PDMS-PMPCS} + \Delta\chi) = \phi(\chi_{PDMS-PMPCS} + |\chi_{PDMS-CO_2} - \chi_{PMPCS-CO_2}|) \quad (1)$$

where ϕ is the volume concentration of the copolymer and $\Delta\chi$ is the absolute value of the difference between PDMS−CO_2 and PMPCS−CO_2 interaction parameters.[10,31]

In order to estimate the ϕ value, we could use the data of the swelling of the PDMS and that of the PMPCS homopolymers in $scCO_2$. The volume change of the copolymer (ΔV) after CO_2 swelling could be calculated as the volume fraction-weighted average of the swelling of the constituent homopolymers[44,45]

$$\Delta V = \phi_{PDMS}\Delta V_{PDMS} + \phi_{PMPCS}\Delta V_{PMPCS} \quad (2)$$

where ΔV_i is the volume change of the constituent homopolymers and ϕ_i is the volume fraction of the *i*th block. Thus, the volume fraction of the block coplymer, ϕ, could be expressed as[45]

Table 3. Morphological Characteristics of $PDMS_{58}$-*b*-$PMPCS_{54}$ and $PDMS_{58}$-*b*-$PMPCS_{75}$ before and after $scCO_2$ Treatment from SAXS Results

sample	q^* (nm^{-1})	*d* (nm)	nanostructure
$PDMS_{58}$-*b*-$PMPCS_{54}$ before $scCO_2$ treatment	0.253	24.8	LAM
$PDMS_{58}$-*b*-$PMPCS_{54}$ after $scCO_2$ treatment	0.244	25.8	LAM
$PDMS_{58}$-*b*-$PMPCS_{75}$ before $scCO_2$ treatment	0.186	33.8	HEX
$PDMS_{58}$-*b*-$PMPCS_{75}$ after $scCO_2$ treatment	0.176	35.7	HEX

$$\phi \approx V_0/(\Delta V + V_0) = V_0/(\xi_{PDMS}\phi_{PDMS}V_0 + \xi_{PMPCS}\phi_{PMPCS}V_0 + V_0) \quad (3)$$

where V_0 is the initial volume of the block copolymer and ξ_i is the ratio of the volume change to the initial volume of the *i*th homopolymer swollen by CO_2 under the same conditions. In $scCO_2$ at 120 °C and 110 bar for 2 h, the ξ_{PDMS} was smaller than 55% as reported in the literature.[46,47] The ξ_{PMPCS} could be estimated from the reported ξ_{PS}. First, the Hildebrand solubility parameter of PMPCS (δ_{PMPCS}) was calculated to be 21.8 $J^{1/2}$ $cm^{-3/2}$ according to the group contribution method.[48] The calculation details are described in the SI. The calculated solubility parameter of PS (δ_{PS}) in the literature is 18.9 $J^{1/2}$ $cm^{-3/2}$.[49] Therefore, ξ_{PMPCS} should be smaller than ξ_{PS}, which was about 7% in $scCO_2$ at 120 °C and 110 bar.[50] For $PDMS_{58}$-*b*-$PMPCS_{66}$, ϕ_{PDMS} was 17.5%, and ϕ_{PMPCS} was 82.5%. As a result, ϕ of $PDMS_{58}$-*b*-$PMPCS_{66}$ at 120 °C and 110 bar should be larger than 86%.

As for comparison of $\chi_{PDMS-PMPCS}$ and $\Delta\chi$, we could calculate them using Hildebrand solubility parameters of the two blocks and $scCO_2$. δ_{PMPCS} was calculated to be 21.8 $J^{1/2}$ $cm^{-3/2}$. The calculated solubility parameter of PDMS (δ_{PDMS}) in the literature is 14.9 $J^{1/2}$ $cm^{-3/2}$.[49] And the solubility parameter of $scCO_2$ (δ_{scCO_2}) has been reported to decrease as pressure decreases or temperature increases.[51] The δ_{scCO_2} value is about 12.2 $J^{1/2}$ $cm^{-3/2}$ at 35 °C and 110 bar, and it decreases to about 3.8 $J^{1/2}$ $cm^{-3/2}$ at 120 °C and 110 bar. On the basis of Flory−Huggins theory, the interaction parameter χ of PMPCS and PDMS blocks could be written in terms of solubility parameter difference as[52,53]

$$\chi_{PDMS-PMPCS} = v_0(\delta_{PMPCS}-\delta_{PDMS})^2/kT \quad (4)$$

where v_0 is the volume per monounit, *k* is the Boltzmann constant, and *T* is temperature in kelvin. For an asymmetric diblock copolymer, v_0 can be replaced by $(v_A v_B)^{1/2}$.[52] v_i, which is the volume of the *i*th monounit, can be calculated as

$$v_i = M_i/(\rho_i N_A) \quad (5)$$

where M_i and ρ_i are the molecular weight of the monounit and the density of the *i*th block, respectively, and N_A is Avogadro's constant. M_i can be obtained from the chemical structure of the block copolymer, and ρ_i values have been given previously. The value of $(v_{PDMS}v_{PMPCS})^{1/2}$ was calculated to be 2.57×10^{-22} cm^{-3}. Therefore,

$$\chi_{PDMS-PMPCS} = 886/T\ (K^{-1}) \quad (6)$$

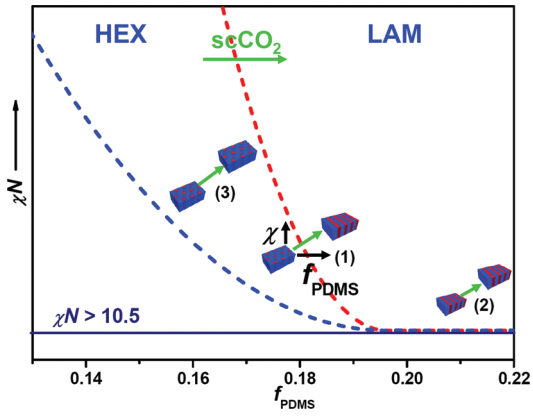

Figure 8. Simplified phase diagram of PDMS-*b*-PMPCS showing the order−order transition of $PDMS_{58}$-*b*-$PMPCS_{66}$ (case 1) and the periodic size changes of $PDMS_{58}$-*b*-$PMPCS_{54}$ (case 2) and $PDMS_{58}$-*b*-$PMPCS_{75}$ (case 3) induced by $scCO_2$.

Thus, at 120 °C, $\chi_{PDMS-PMPCS}$ was ~2.25, and at 160 °C, $\chi_{PDMS-PMPCS}$ was about 2.05.

The polymer−solvent Flory−Huggins parameter χ could also be calculated using the Hildebrand solubility parameter approach,[9] which gave

$$\chi_{polymer-solvent} = V(\delta_{polymer} - \delta_{solvent})^2/RT + b \quad (7)$$

where V is the molar volume of the solvent, $\delta_{polymer}$ and $\delta_{solvent}$ are the solubility parameters of the polymer and the solvent, respectively, R is the gas constant, T is the temperature in kelvin, and b is a constant. Thus, $\Delta\chi$ could be expressed as

$$\Delta\chi = |\chi_{PDMS-CO_2} - \chi_{PMPCS-CO_2}| = |V[(\delta_{PMPCS} + \delta_{PDMS} - 2\delta_{scCO_2})(\delta_{PMPCS} - \delta_{PDMS})]/RT| \quad (8)$$

The δ_{scCO_2} value and the density of $scCO_2$ (ρ_{scCO_2}) decrease[54] as temperature increases at the same pressure. Therefore, $\Delta\chi$ increased as temperature increased. At 35 °C and 110 bar, δ_{scCO_2} value is about 12.2 $J^{1/2}$ $cm^{-3/2}$, ρ_{scCO_2} is 0.71 g/cm^3, and $\Delta\chi$ was about 2.04. At 120 °C and 110 bar, δ_{scCO_2} value is about 3.8 $J^{1/2}$ $cm^{-3/2}$, ρ_{scCO_2} is 0.18 g/cm^3, and $\Delta\chi$ was about 16.9.

Consequently, when the sample was treated in $scCO_2$ at 120 °C and 110 bar, ϕ was larger than 0.86, $\chi_{PDMS-PMPCS}$ was 2.25, and $\Delta\chi$ was large and dominated the contribution to χ_{eff}. Moreover, $\chi_{PDMS-PMPCS}$ was larger at 120 °C than at 160 °C. These three factors resulted in an increased χ_{eff} which promoted the phase transition.

Thus, increases in both the volume fraction of PDMS and χ contributed to the order−order transition. Additionally, the sorption of $scCO_2$ increased the chain mobility, allowing the transition to achieve in a short time. When $scCO_2$ was released slowly at the temperature lower than the effective T_g of PMPCS in $scCO_2$, the rigid PMPCS block fixed the lamellar structure. From the phase behavior following $scCO_2$ treatment of PDMS-*b*-PMPCS, we could use a simplified phase diagram to explain the experimental results as shown in Figure 8, although the changes/transitions were for BCP−$scCO_2$ mixtures instead of pure BCPs in bulk. Whether an OOT could take place depended on the location of the original phase in the phase diagram and the magnitude of changes in f_{PDMS} and χ.

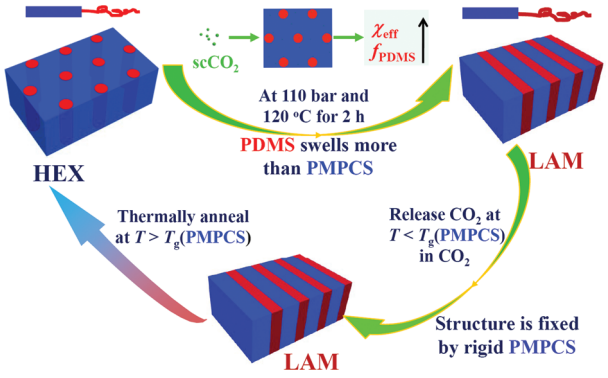

Figure 9. Schematic representation of the proposed mechanism of the HEX−LAM transition of $PDMS_{58}$-*b*-$PMPCS_{66}$ induced by $scCO_2$.

Mechanism of the $scCO_2$-Induced Order−Order Transition in $PDMS_{58}$-*b*-$PMPCS_{66}$. On basis of these results, we concluded that because the preferential swelling increased the volume fraction of the CO_2-philic block and the difference in the interactions of the two blocks with CO_2 as well as the relatively low temperature during $scCO_2$ treatment increased the effective interaction parameter, $scCO_2$ induced the HEX−LAM transition of $PDMS_{58}$-*b*-$PMPCS_{66}$. This is an excellent method to induce OOTs for BCPs containing a CO_2-philic block and control the nanostructure. The philicity of the PDMS block with CO_2 was important for the transition upon swelling, while the rigidity of PMPCS was important for fixation of the final structure. In addition, the gaseous nature of CO_2 at ambient conditions rendered CO_2 its advantages as a fast-releasing swelling agent, which also helped fix the structure. The lamellae could revert to hexagonally packed cylinders, which was the stable structure under this condition, through thermal annealing. Figure 9 shows the proposed mechanism of the OOTs. For other BCPs containing CO_2-philic fluoropolymers and polysilicones, this method may also be useful for further research.

CONCLUSIONS

In summary, we have synthesized a series of well-defined PDMS-*b*-PMPCS rod−coil BCPs with a CO_2-philic coil block and a CO_2-phobic rod block through ATRP and studied their phase behavior in bulk and in $scCO_2$ of relatively low pressures. The nanostructures of the BCPs changed from LAM to HEX as f_{PDMS} decreased. For $PDMS_{58}$-*b*-$PMPCS_{66}$ which was located close to the HEX−LAM phase boundary in the phase diagram under our experimental conditions, the SAXS results on $scCO_2$-treated, originally amorphous samples indicated the formation of lamellar structures rather than hexagonally packed cylinders. In treating $PDMS_{58}$-*b*-$PMPCS_{66}$ having the structure of hexagonally packed cylinders with $scCO_2$, we found that $scCO_2$ could induce the order−order transition of this sample. Supercritical CO_2 could swell the CO_2-philic block more and improve the ordering kinetics of BCPs. The OOT in PDMS-*b*-PMPCS was ascribed to increases in both f_{PDMS} and χ_{eff}. The final LAM structure was stable below the high T_g of the rod block and could revert to the HEX structure by thermal annealing above the T_g of the rod block. For other BCPs located far away from the HEX−LAM phase boundary in the phase diagram, the structures did not change, but the periodic sizes increased following $scCO_2$ treatment. The approach described in this work is convenient and environmentally friendly. We are currently exploring more

details about the effect of $scCO_2$ on the self-assembly of this diblock copolymer system. Furthermore, in these PDMS-*b*-PMPCS BCPs, PDMS not only is CO_2-philic but also has low surface energy. Therefore, the self-assembling behavior of PDMS-*b*-PMPCS thin films on different substrates in $scCO_2$ will also be interesting. To this end, further research is in progress.

■ ASSOCIATED CONTENT

Supporting Information. Text and tables about the Hildebrand solubility parameter of PMPCS and densities of the BCP samples before and after $scCO_2$ treatment; figures and tables showing some characterization results of the macroinitiator and PDMS-*b*-PMPCS block copolymers. This material is available free of charge via the Internet at http://pubs.acs.org.

■ AUTHOR INFORMATION

Corresponding Author

*E-mail: zshen@pku.edu.cn (Z.S.); fanxh@pku.edu.cn (X.-H.F.).

■ ACKNOWLEDGMENT

Financial support from the National Natural Science Foundation of China (Grant 20874003) is gratefully acknowledged. The authors also thank Dr. M. Q. Ren at Beijing Research Institute of Chemical Industry for the assistance with the SAXS measurements.

■ REFERENCES

(1) Muthukumar, M.; Ober, C. K.; Thomas, E. L. *Science* **1997**, *277*, 1225–1232.
(2) Ikkala, O.; ten Brinke, G. *Science* **2002**, *295*, 2407–2409.
(3) Bates, F. S.; Fredrickson, G. H. *Phys. Today* **1999**, *52*, 32.
(4) Ruzette, A.-V.; Leibler, L. *Nature Mater.* **2005**, *4*, 19–31.
(5) Lodge, T. P. *Macromol. Chem. Phys.* **2003**, *204*, 265–273.
(6) Matsen, M. W.; Bates, F. S. *Macromolecules* **1996**, *29*, 1091–1098.
(7) Chen, J. T.; Thomas, E. L.; Ober, C. K.; Mao, G. P. *Science* **1996**, *273*, 343–346.
(8) Tenneti, K. K.; Chen, X.; Li, C. Y.; Tu, Y.; Wan, X.; Zhou, Q.-F.; Sics, I.; Hsiao, B. S. *J. Am. Chem. Soc.* **2005**, *127*, 15481–15490.
(9) Liu, Y. S.; Li, M. H.; Bansil, R.; Steinhart, M. *Macromolecules* **2007**, *40*, 9482–9490.
(10) Lodge, T. P.; Pudil, B.; Hanley, K. J. *Macromolecules* **2002**, *35*, 4707–4717.
(11) Hanley, K. J.; Lodge, T. P.; Huang, C. I. *Macromolecules* **2000**, *33*, 5918–5931.
(12) Roe, R. J.; Zin, W. C. *Macromolecules* **1984**, *17*, 189–194.
(13) Gao, L.; Yao, J.; Shen, Z.; Wu, Y.; Chen, X.; Fan, X.; Zhou, Q. *Macromolecules* **2009**, *42*, 1047–1050.
(14) Huang, Y.-Y.; Hsu, J.-Y.; Chen, H.-L.; Hashimoto, T. *Macromolecules* **2007**, *40*, 3700–3707.
(15) Kimishima, K.; Koga, T.; Hashimoto, T. *Macromolecules* **2000**, *33*, 968–977.
(16) Yoon, J.; Jin, S.; Ahn, B.; Rho, Y.; Hirai, T.; Maeda, R.; Hayakawa, T.; Kim, J.; Kim, K. W.; Ree, M. *Macromolecules* **2008**, *41*, 8778–8784.
(17) Ly, D. Q.; Honda, T.; Kawakatsu, T.; Zvelindovsky, A. V. *Macromolecules* **2007**, *40*, 2928–2935.
(18) Schmidt, K.; Schoberth, H. G.; Ruppel, M.; Zettl, H.; Hansel, H.; Weiss, T. M.; Urban, V.; Krausch, G.; Boker, A. *Nature Mater.* **2008**, *7*, 142–145.
(19) Hong, Y.-R.; Adamson, D. H.; Chaikin, P. M.; Register, R. A. *Soft Matter* **2009**, *5*, 1687–1691.
(20) Urbas, A.; Sharp, R.; Fink, Y.; Thomas, E. L.; Xenidou, M.; Fetters, L. J. *Adv. Mater.* **2000**, *12*, 812–814.
(21) Schmidt, K.; Pester, C. W.; Schoberth, H. G.; Zettl, H.; Schindler, K. A.; Böker, A. *Macromolecules* **2010**, *43*, 4268–4274.
(22) Anastas, P. T.; Kirchhoff, M. M. *Acc. Chem. Res.* **2002**, *35*, 686–694.
(23) Kaiser, J. *Science* **1996**, *274*, 2013–2010.
(24) Desimone, J. M.; Guan, Z.; Elsbernd, C. S. *Science* **1992**, *257*, 945–947.
(25) Cain, J. B.; Zhang, K.; Betts, D. E.; DeSimone, J. M.; Johnson, C. S. *J. Am. Chem. Soc.* **1998**, *120*, 9390–9391.
(26) Wissinger, R. G.; Paulaitis, M. E. *J. Polym. Sci., Part B: Polym. Phys.* **1991**, *29*, 631–633.
(27) RamachandraRao, V. S.; Gupta, R. R.; Russell, T. P.; Watkins, J. J. *Macromolecules* **2001**, *34*, 7923–7925.
(28) Watkins, J. J.; Brown, G. D.; RamachandraRao, V. S.; Pollard, M. A.; Russell, T. P. *Macromolecules* **1999**, *32*, 7737–7740.
(29) Vogt, B. D.; Brown, G. D.; RamachandraRao, V. S.; Watkins, J. J. *Macromolecules* **1999**, *32*, 7907–7912.
(30) Vogt, B. D.; RamachandraRao, V. S.; Gupta, R. R.; Lavery, K. A.; Francis, T. J.; Russell, T. P.; Watkins, J. J. *Macromolecules* **2003**, *36*, 4029–4036.
(31) Li, Y.; Wang, X. C.; Sanchez, I. C.; Johnston, K. P.; Green, P. F. *J. Phys. Chem. B* **2007**, *111*, 16–25.
(32) Arceo, A.; Green, P. F. *J. Phys. Chem. B* **2005**, *109*, 6958–6962.
(33) Yokoyama, H.; Sugiyama, K. *Macromolecules* **2005**, *38*, 10516–10522.
(34) Taki, K.; Waratani, Y.; Ohshirna, M. *Macromol. Mater. Eng.* **2008**, *293*, 589–597.
(35) Yokoyama, H.; Li, L.; Dutriez, C.; Iwakura, Y.; Sugiyama, K.; Masunaga, H.; Sasaki, S.; Okuda, H. *Macromolecules* **2008**, *41*, 8626–8631.
(36) Li, L.; Nemoto, T.; Sugiyama, K.; Yokoyama, H. *Macromolecules* **2006**, *39*, 4746–4755.
(37) Zhang, R.; Yokoyama, H. *Macromolecules* **2009**, *42*, 3559–3564.
(38) Li, L.; Yokoyama, H. *Angew. Chem., Int. Ed.* **2006**, *45*, 6338–6341.
(39) Zhang, D.; Liu, Y.-X.; Wan, X.-H.; Zhou, Q.-F. *Macromolecules* **1999**, *32*, 5183–5185.
(40) Ye, C.; Zhang, H. L.; Huang, Y.; Chen, E. Q.; Lu, Y. L.; Shen, D. Y.; Wan, X. H.; Shen, Z. H.; Cheng, S. Z. D.; Zhou, Q. F. *Macromolecules* **2004**, *37*, 7188–7196.
(41) Hashimoto, T.; Kawamura, T.; Harada, M.; Tanaka, H. *Macromolecules* **1994**, *27*, 3063–3072.
(42) Ryan, A. J.; Hamley, I. W.; Bras, W.; Bates, F. S. *Macromolecules* **1995**, *28*, 3860–3868.
(43) Guan, Y.; Chen, X. F.; Ma, H. Y.; Shen, Z. H.; Wan, X. H. *Soft Matter* **2010**, *6*, 922–927.
(44) Francis, T. J.; Vogt, B. D.; Wang, M. X.; Watkins, J. J. *Macromolecules* **2007**, *40*, 2515–2519.
(45) Chang, S. H.; Park, S. C.; Shim, J. J. *J. Supercrit. Fluids* **1998**, *13*, 113–119.
(46) Garg, A.; Gulari, E.; Manke, C. W. *Macromolecules* **1994**, *27*, 5643–5653.
(47) Royer, J. R.; DeSimone, J. M.; Khan, S. A. *Macromolecules* **1999**, *32*, 8965–8973.
(48) Barton, A. F. M. In *Handbook of Solubility Parameters and Other Cohesion Parameters*; CRC Press: Boca Raton, FL, 1983.
(49) Barton, A. F. M. In *Handbook of Polymer-Liquid Interaction Parameters and Solubility Parameters*; CRC Press: Boca Raton, FL, 1990; pp 125−147.
(50) Hilic, S.; Boyer, S. A. E.; Padua, A. A. H.; Grolier, J. P. E. *J. Polym. Sci., Part B: Polym. Phys.* **2001**, *39*, 2063–2070.
(51) Allada, S. R. *Ind. Eng. Chem. Process Des. Dev.* **1984**, *23*, 344–348.
(52) Hashimoto, T.; Shibayama, M.; Kawai, H. *Macromolecules* **1980**, *13*, 1237–1247.
(53) Kim, B.; Kim, J.; Jung, B. *J. Membr. Sci.* **2005**, *250*, 175–182.
(54) Span, R.; Wagner, W. *J. Phys. Chem. Ref. Data* **1996**, *25*, 1560–1593.